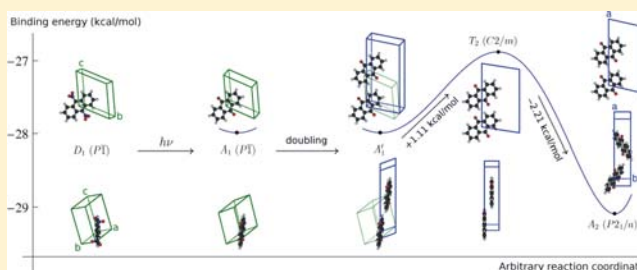# Crystal-to-Crystal Photoinduced Reaction of Dinitroanthracene to Anthraquinone

Tommaso Salzillo, Ivano Bilotti, Raffaele Guido Della Valle, Elisabetta Venuti, and Aldo Brillante*

Dipartimento di Chimica Fisica e Inorganica and INSTM−UdR Bologna, University of Bologna, I-40136 Bologna, Italy

S *Supporting Information*

ABSTRACT: The photochemical reaction of 9,10-dinitroan-thracene (DNO_2A) to anthraquinone (AQ) + 2NO has been studied by means of lattice phonon Raman spectroscopy in the spectral region $10-150$ cm^{-1}. In fact, crystal-to-crystal transformations are best revealed by following changes in the lattice modes, as even small modifications in the crystal structure lead to dramatic changes in symmetry and selection rules of vibrational modes. While analysis of the lattice modes allowed for the study of the physical changes, the chemical transformation was monitored by measuring the intra-molecular Raman-active modes of both reactant and product. On the basis of the experimental data it has been possible, at a microscopic level, to infer crucial information on the reaction mechanism by simultaneously detecting molecular (vibrational modes) and crystal structure (lattice phonons) modifications during the reaction. At a macroscopic level we have detected an intriguing relationship between incident photons and mechanical strain, which manifests itself as a striking bending and unfolding of the specimens under irradiation. To clarify the mechanisms underlying the relationship between incoming light and molecular environment, we have extended the study to high pressure up to 2 GPa. It has been found that above 1 GPa the photoreaction becomes inhibited. The solid-state transformation has also been theoretically modeled, thus identifying the reaction pathway along which the DNO_2A crystal lattice deforms to finally become the crystal lattice of the AQ product.

1. INTRODUCTION

Crystal-to-crystal reactions represent a unique stage of play for a number of cooperative phenomena involving structure and dynamics of the lattice. The energetic cost needed to evolve to products requires a large structural reconstruction of the lattice of the reactant, which is often reached with the help of high temperature or high pressure. When the chemical and physical transformations are driven by photons, molecular displace-ments follow light absorption, which promotes chemical changes according to the relative positions and orientations of the molecules in the crystal structure. The energy transfer and the chemical reaction itself are then favored by the ordered structure of the crystal, and the lattice becomes the actual cage where the photoreaction takes place.[1] Its counterpart in solution is the perfect fit of dimerized molecules in a confined environment.[2]

The second aspect of photoreactions in the solid state is the transformation of the photon energy in new forms, capable of driving the chemical and the physical changes. The most spectacular one is the mechanical motion obtained in response to absorption of light, which manifests as a movement at the supramolecular level (molecular machines)[3−5] or of the entire crystal (photomechanical actuators).[6−10]

Most recently Bardeen and co-workers have reported a reversible twisting of microribbons of 9-anthracenecarboxylic acid resulting from its photodimerization.[11] Their analysis of the experimental data suggests that crystal motion is generated by the interfacial strain within the crystal between unreacted monomer and photoreacted dimer regions.

Given this background, we have studied the crystal-to-crystal photoreaction of 9,10-dinitroanthacene (hereafter indicated as DNO_2A) to anthraquinone (AQ) + 2NO. The reaction has been previously observed in solution,[12] and its mechanism has been recently revisited,[13] but it reveals intriguing aspects when performed by irradiation of the single crystal. In fact, the reaction path requires a striking modification of the crystal lattice, starting from the triclinic structure of DNO_2A, with one molecule per unit cell (Z = 1), to yield the monoclinic structure of AQ with Z = 2. Indeed, this involves a considerable change of the chemical environment, which implies the use of sensitive probes of intermolecular interactions. For our investigation, we have used the novel approach of following the reaction by means of lattice phonon Raman microscopy,[14] a technique that directly probes intermolecular modes, i.e., collective transla-tional or rotational motions of the molecules in the unit cell. These modes produce dynamical deformations of the crystal called lattice vibrations or lattice phonons, whose frequencies, resulting in Raman shifts in the range $\sim10-150$ cm^{-1}, are very sensitive to even slightly different molecular packing. Raman spectroscopy in the energy range of molecular vibrations has been successfully applied to follow solid-state reactions,[15,16]

while Prasad and co-workers had previously investigated also the role of lattice phonons.[17,18] Our approach combines microscopy and Raman spectroscopy with the additional advantage of confocality. This has allowed us to follow the evolution of the photoreaction *in situ*, yielding the Raman signal at a spatial resolution below 1 μm. Crystal and molecular spectral changes were compared with the optical images of the sample.

While the analysis of the lattice modes allowed for the study of the physical changes (lattice dynamics), the chemical transformation was monitored by measuring the intramolecular Raman-active modes of both reactant and product, on the very same spot at the same time.

The experiments show that, once triggered, the reaction proceeds rapidly until a complete transformation to the product. The change in crystal morphology strongly depends upon the different conditions of irradiation and on sample history. In any case, the irradiated crystals undergo impressive mechanical movements which manifest themselves as striking bending and unfolding of the specimens under irradiation.

We have extended the study to high pressure, up to 2 GPa. It has been found that above 1 GPa the photoreaction becomes inhibited.

Finally, lattice dynamics methods were used to describe the crystal-to-crystal transformation which takes place through a complex cell doubling mechanism. The computational approach has allowed us to select the best candidate structure for the transition state in the pathway linking reactant and product lattices.

2. EXPERIMENTAL SECTION

Single crystals of DNO$_2$A were grown by sublimation of commercial material from Aldrich. The most common morphology is that of needles elongated along the *a* axis.

Lattice phonon spectra were obtained by placing the sample on the optical stage of an optical microscope (Olympus BX40) interfaced to a Jobin Yvon T64000 Raman spectrometer, with 50× or 100× objectives, which allowed us to obtain a spatial resolution just below 1 μm and a *theoretical* field depth ranging from about 7 to 25 μm. Spectra were recorded spanning the low wavenumber region of the lattice phonons (10−150 cm^{-1}). The excitation wavelength was from a krypton laser tuned at 647.1 nm, an excitation energy sufficiently low to avoid both background fluorescence from the sample and its photochemical change. The incoming power was reduced with a neutral filter whose optical density was selected in each experiment to prevent crystal damage, the actual power focused on the sample being anyway less than 1 mW. Intramolecular vibrations of both DNO$_2$A and AQ were detected in the range 400−1800 cm^{-1}. For more details on the spectroscopic characterization, see ref 14.

Two different procedures were followed to irradiate the crystal, i.e., broadband and laser photoexcitations. For the former, a 75 W Xe lamp was used, and the spectral range ∼250−400 nm was selected with a glass filter. Laser excitation was instead produced by a 25 mW diode laser tuned at 405 nm.

High-pressure measurements were performed in different high-pressure cells with sapphire windows (0−0.1 GPa) or diamond anvils (>1 GPa). A 4:1 methanol−ethanol solution was used as hydrostatic medium, and pressures were calibrated with the ruby fluorescence method.[19]

3. RESULTS

3.1. Lattice Phonon Raman Spectra. The first step to conveniently follow the photoreaction is to set the reference data of pure reactant and product. The lattice phonon Raman spectrum of DNO$_2$A and AQ are both known from the literature.[20,21] For a convenient comparison, we report in Figure 1 the ambient (*p,T*) spectra of the actual samples used in the experiments.
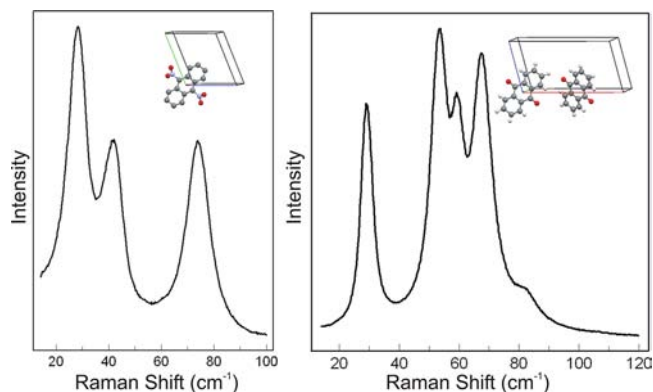

Figure 1. Lattice phonon Raman spectra of (left) DNO$_2$A and (right) AQ. The corresponding molecules in the unit cell are reported in the insets.

The crystal structure of DNO$_2$A is triclinic $P\bar{1}$ (C_i^1) with one molecule per unit cell.[22] Since $Z = 1$, only three **k** = 0 optical lattice phonons are present and are of A_g symmetry, i.e., Raman-active.[23] They are all shown in Figure 1. The crystal structure of AQ is monoclinic $P2_1/a$ (C_{2h}^5) with two molecules per unit cell.[24,25] Since $Z = 2$, nine **k** = 0 optical lattice phonons are allowed, and six ($3A_g + 3B_g$) are Raman-active.[23] Five out of the six[21] are shown in Figure 1.

3.2. Crystal-to-Crystal Photoreaction of DNO$_2$A to AQ. Although studied in solution, no reports can be found in the literature of this reaction in the solid state. When the reaction is performed by photoexcitation of the crystal, the initial step, following light absorption, is the localization of the exciton in active sites, usually physical traps, which act as nucleation centers for the its propagation throughout the entire crystal. In this sense solid-state photoreactions can be classified as cooperative. Selectivity and localization are then the dominant factors of the process.[1]

A collective propagation of the excited reactant molecules into the product must necessarily follow the rule governing ordered systems, that is, a topochemical principle or the capability of the reactant molecules to be in the correct registry to yield the product with a minimum of orientational reconstruction. Crystal packing, in other words, already has the capability of determining the chemical change produced by incoming light.[26,27] A historical survey of the early experiments on the subject can be found in the literature.[28] A remarkable variant to the topochemical principle can be found when the reaction starts in defective sites of crystals lacking perfect crystalline order, such as, for instance, the photodimerization of 9-cyanoanthracene.[1] In this case the reaction is triggered by defects.

3.2.1. Broadband Excitation. Single crystals of DNO$_2$A were irradiated by a Xe lamp with UV excitation in the range ∼250−400 nm selected by a glass filter (radiative flux 5 × 10^{-5} W/cm^2). A water filter was placed in the optical path to prevent sample heating which can damage the crystal and lead to formation of secondary products. Lattice phonon Raman spectra were recorded as a function of time to monitor the photoreaction. The UV excitation was focused on one end only of the single crystal, in order to compare reacted and unreacted

regions on the same specimen. Figure 2 reports the sample morphology and the Raman spectra collected at regular time
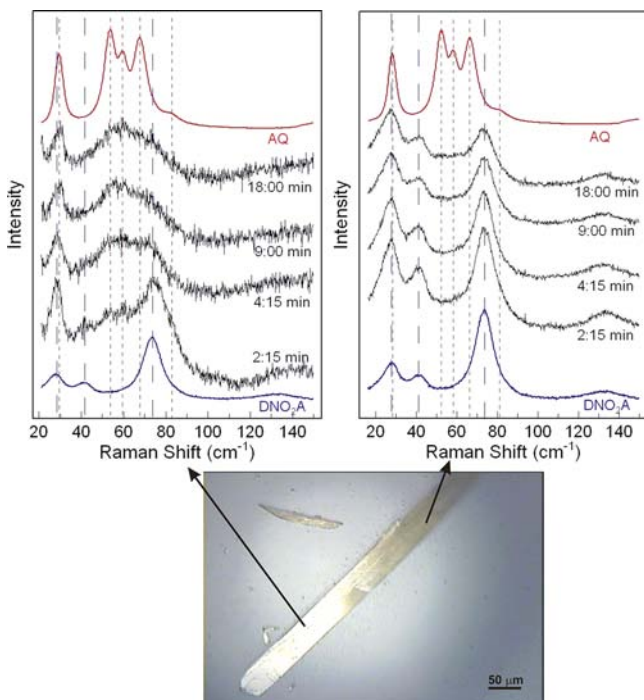

Figure 2. Lattice phonon Raman spectra of (left) irradiated and (right) non-irradiated regions of a DNO$_2$A single crystal, shown below. In the upper part of the figures, the spectrum of the single crystal of AQ is reported as reference.

intervals. As a reference, the phonon spectrum of pure AQ is reported at the top of the figures. After only 2 min, a marked color difference has been observed between the two ends of the sample. Correspondingly, Raman profiles of the illuminated region show the fast growth of AQ lattice phonons which initially overlap the phonon bands of the starting DNO$_2$A crystal and eventually fully replace them. The right side of the figure shows only the phonon bands of DNO$_2$A in the region of

the sample not subjected to irradiation. The reaction quickly proceeds to completion after only 4 min. We remark that the reaction is not limited to the surface area of the specimen. In fact, the presence of AQ molecules into the bulk of DNO$_2$A crystal was confirmed by changing the microscope objectives from 100× to 10×, corresponding to a theoretical range of field depth from 7.5 to 450 μm.

Completion of the reaction over the entire crystal was further proved by mass spectra, which showed no residual signal of the reactant. The resulting phonon spectrum of the photoproduct shows broader bands with respect to those of a pure pristine single crystal AQ (red trace in Figure 2). This can be accounted for by the inhomogeneuos broadening induced by local disorder in the photoproduct.

3.2.2. Laser Excitation. A focused beam from a 25 mW diode laser tuned at 405 nm (radiative flux 340 W/cm^2) unfailingly produced an immediate and explosive breaking of the crystal. The experiments were then performed with a series of variable optical density filters attenuating the incoming light up to 3 orders of magnitude, which resulted in an increase in the time required to complete the reaction in the order of hours. Results are reported in Figure 3. Although slower, the modification of the lattice is accompanied by a gradual change of the whole phonon spectrum from the lattice modes of pure crystalline DNO$_2$A to those of pure AQ. The better control of the photoreaction can also be deduced by the absence of any background fluorescence, whose presence would certainly be an indication of the formation of secondary photoproducts, acting as emitting impurity traps. The pictures of the crystal in the right-hand side of Figure 3 show that in any case, although less dramatically, the crystal that is initially a few hundreds micrometers long breaks up in a number of fragments at the end of the reaction (t = 530 min). The large mechanical strain, which starts in the middle point of crystal where the laser beam is focused, obviously produces this destructive process. The post analysis of the Raman spectra of these fragments indicates that they certainly belong to pure AQ (upper spectrum of the Figure), an indication that the reaction had indeed reached its full completion. Unlike the spectra of figure 2, all phonon bands
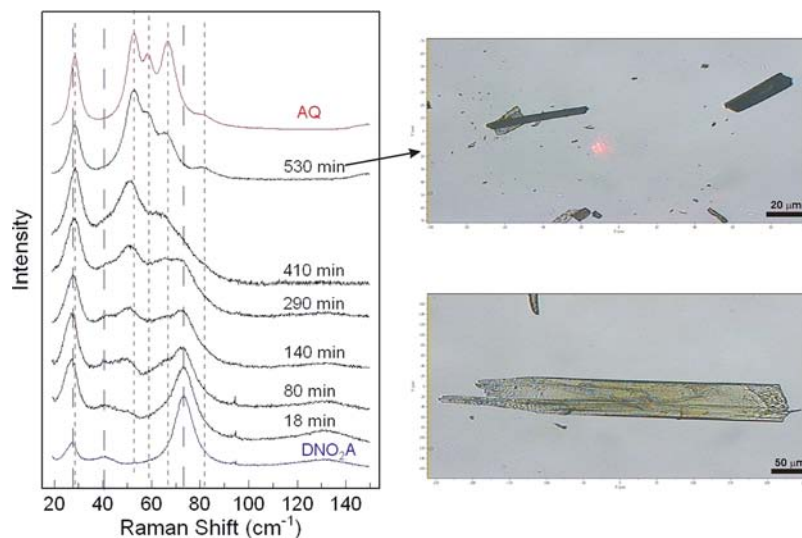

Figure 3. (Left) Lattice phonon Raman spectra of a DNO$_2$A single crystal as a function of time (UV irradiaton from a focused laser). (Right) Pictures of the crystal before (bottom) and after (top) the photoreaction.
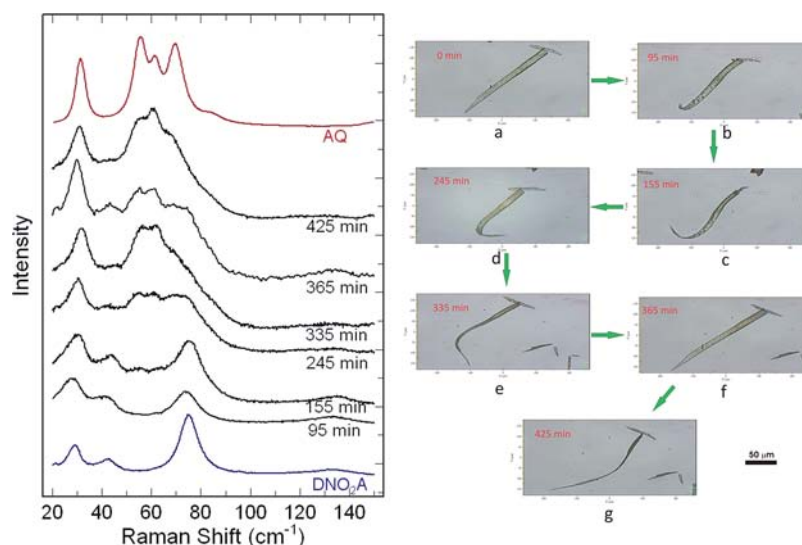
Figure 4. (Left) Lattice phonon Raman spectra of a DNO_2A single crystal as a function of time under uniform irradiaton from a defocused UV laser beam. (Right) Snapshots, at the corresponding times, of the irradiated crystal during the course of the reaction.
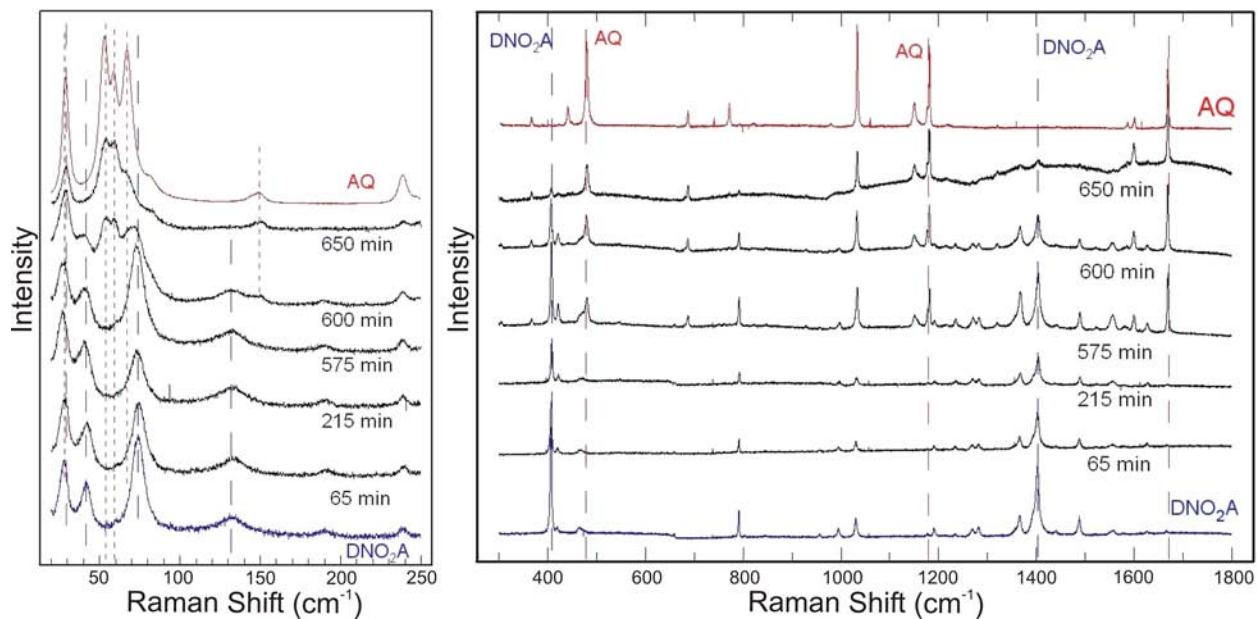

Figure 5. (Left) Lattice phonon Raman spectra and (right) internal vibration spectra in the region $300-1800$ cm^{-1} at different times of irradiation of a single crystal of DNO_2A.

are well resolved and compare well to those of the reference single crystal spectrum of AQ.

To avoid the fragmentation of the crystal, we defocused the laser beam on the crystal surface to get a more controlled and uniform irradiation (radiative flux 3×10^{-2} W/cm^2), an expedient also used to control the interfacial strain in the photodimerization of 9-anthracenecarboxylic acid.[11] Indeed, under these conditions, the mechanical deformation of the crystal during the progress of the photoreaction is always homogeneously distributed over the entire size of the crystal, avoiding its destructive fragmentation. It looks as if the macroscopic boundaries of the crystal, edges and surface, soften the strain produced by photons. One of the most intriguing results obtained under these experimental conditions is shown in Figure 4.

Here the photoreaction completes pretty much in the same time scale as that of the previous experiment where, though attenuated, the laser beam was focused on the crystal. However, now the starting crystal avoids breaking into smaller fragments and undergoes after irradiation a striking series of mechanical movements, which result in bending, twisting and unfolding, as shown in the right side of the figure. The well-shaped single crystal (a) initially bends, especially at one of its ends (b−c), then rotates by 180° along the stack axis to reach, after the unfolding (d) and further twisting (e), its initial shape (f). The transformation is not complete, as indicated by the spectral profiles after 365 min, where residual phonon bands of DNO_2A lattice are still present. The final step, up to the complete formation of AQ, requires a new and fast deformation of the crystal, as explained in section 3.4. This eventually leads to pure AQ (g), the phonon bands of which undergo a minor

broadening, as shown by the congested region around 60 cm^{-1}. A different intensity spectral distribution with respect to that of the reference crystal can be accounted for by an orientational change of the anisotropic crystal formed after irradiation. Similar trends have been observed for other crystals of approximately the same shape and size. A short movie documenting this spectacular behavior can be found in the Supporting Information.

During the course of the photoreaction, the extensive study of the Raman phonon spectra (changes of the lattice) has been completed by the simultaneous detection of the intramolecular modes (molecular modifications), in order to compare the molecular transformation of DNO$_2$A to AQ with the corresponding changes of the crystal lattice (from triclinic to monoclinic). This investigation is crucial for the determination of the reaction mechanism following the photon absorption. Figure 5 shows these data.

Quite interestingly, at reaction times for which no remarkable variations in the lattice phonon spectrum have been observed, the internal vibrations of molecular AQ are already well visible, as can be seen in Figure 5, where sample bands have been marked by vertical lines. The relative intensities of the bands at 1403 and 1675 cm^{-1}, corresponding to intramolecular modes for DNO$_2$A and AQ, respectively, have been analyzed at a time (575 min) where the lattice still appears to be as that of pure triclinic DNO$_2$A crystal. Taking into account the *ab initio* value of the Raman intensities calculated for the isolated molecules (from the calculations of section 4), we can estimate that about 40% of DNO$_2$A has already reacted at this time and therefore a surprisingly large amount of AQ is already present. In other words, it is as though the photoproduct AQ occupies substitutional sites of the triclinic lattice of DNO$_2$A; i.e., the molecular transformation by far precedes the transformation of the crystal lattice, an important finding that will be discussed in section 4.

3.3. Photochemical Reaction at High Pressure.
Pressure is a most efficient tool for the perturbation of intermolecular interactions, though leaving basically unchanged the molecular environment. Since large mechanical strains are undoubtedly involved in the crystal-to-crystal transformation of DNO$_2$A to AQ, we have investigated the reaction as a function of pressure to get further hints on its mechanism. Pressure is a very sensitive probe of molecular interactions and it seems therefore appropriate to use it in a transformation where incoming light and molecular constraints play a crucial role on the route to the photoproduct.

Several measurements have been performed over a wide pressure range and different irradiation conditions. We limit the description of the experiment to a few typical cases, one of which is illustrated in Figure 6. More experiments are reported as Supporting Information. Here the crystal has been irradiated by the diode laser at 405 nm and has been subjected to a constant pressure of 0.7 GPa in a gasketed diamond anvil cell (DAC). Changes of the crystal morphology have been simultaneously detected at constant time intervals.

After 80 min the reaction reaches its full completion in the irradiated region, and the observed phonon bands are uniquely attributed to AQ lattice vibrations. It is of some interest to follow the changes of the shape of the crystal during the reaction. Although the crystal is subjected to the strong mechanical strain induced by the incoming light, it is nevertheless constrained in the gasket area, which produces a sort of physical barrier in limiting the sample movement. The
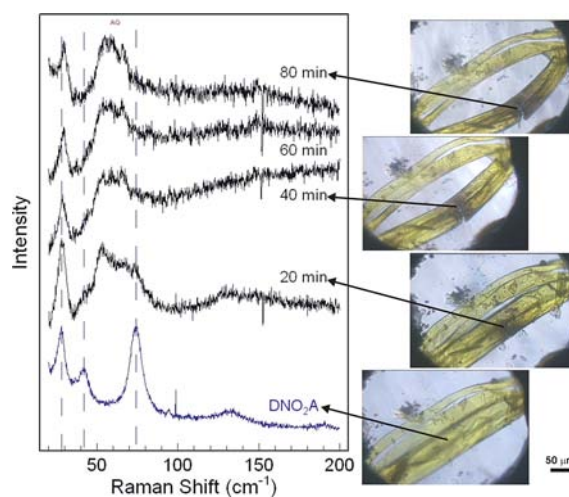

Figure 6. (Left) Lattice phonon Raman spectra at p = 0.7 GPa. (Right) Corresponding changes in crystal morphology at constant time intervals.

crystal bends and curiously forms a sort of ring at the point where the focused laser light, strongly attenuated by optical density filters, had started the photoreaction. By further increasing the pressure to about 1 GPa, a process similar to that described in Figure 7 occurs. Eventually, above 1 GPa and
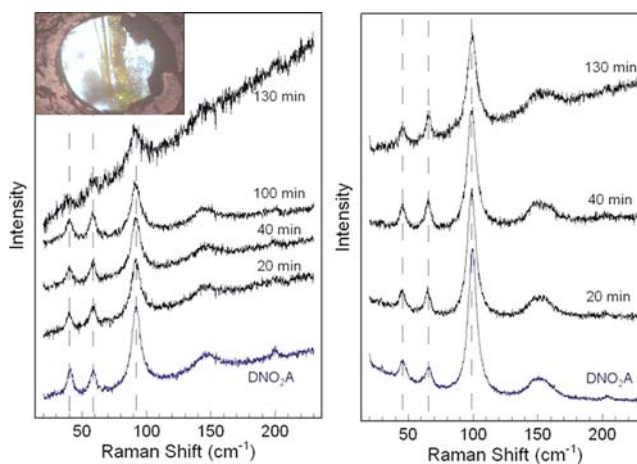

Figure 7. Lattice phonon Raman spectra of a crystal irradiated at (left) 1.0 and (right) 1.4 GPa. Inset: picture of the irradiated crystal at 1.0 GPa.

irrespective of prolonged irradiation, no transformation to AQ occurs, as shown in Figures 7 and SI-1 (Supporting Information). Besides, the very same DNO$_2$A crystal that went unreacted at 1.4 GPa completely transforms to AQ after 20 min after the pressure was released to 0.4 GPa (Figure SI-2). The complete absence of molecular modes of AQ (Figure SI-3) confirms that the reaction has not started at either the physical or chemical level. The picture of the crystal correspondingly changes, showing that, although it undergoes a longitudinal fracture under pressure and light, it never bends. It seems as though the release of the mechanical energy (revealed by the crystal motion) is indeed the driving force required for the advancement of the photoreaction.

Examples of photochemical dimerizations inhibited at high pressures can be found in some experiments a few decades old.[29,30] We believe that the most important factor which can

explain the inhibition of the reaction at high pressure is that the release of NO cannot take place if the external pressure is too high.

3.4. Progress of the Reaction. We describe the following steps to advance a plausible hypothesis on the evolution of the reaction as shown by the experiments.

3.4.1. Triggering the Reaction. The trigger of the reaction occurs through a well-known mechanism for photochemical reactions in organic crystals.[1,28] Following light absorption, a delocalized exciton (*ideal crystal*) forms, which eventually localizes (*real crystal*) into chemical or physical traps of the crystal. These traps are sites of local disorder that become the *active sites*, that is, the nucleation centers which trigger the photoreaction. The transformation in these local sites of molecules of DNO_2A to AQ provides further disorder, increasing the number of active sites capable of driving the reaction. The reaction starts, and as long as DNO_2A molecules continue to transform to AQ, the latter, being in a foreign lattice, creates further trapping sites which favor the course of the reaction, following a collective autocatalytic mechanism.

3.4.2. Chemical Reaction in a Cage: The Cage Is the Unit Cell. Once the reaction has been triggered, the ordered structure of the crystal is the dominating factor for its propagation. By looking at the crystal parameters of DNO_2A and AQ (Table 1, section 4), it is tempting to think of a simple reaction mechanism mostly based on a cell doubling, in a direction that could be the *b* or *c* axis, or a more complicated combination of axes. This would result in a convenient topochemical path to justify how the reaction easily completes, starting from the triclinic cell (Z = 1) of DNO_2A to get the monoclinic cell (Z = 2) of AQ with about double the volume. The triclinic unit cell of DNO_2A can thus be considered as the chemical cage where the photoreaction begins.[1]

The reaction path leading to the cell doubling is computationally modeled in section 4.

3.4.3. Propagation of the Reaction: From the Cage to the Whole Crystal. The information on the crystal structure obtained through the Raman phonon spectra gives some hints on the progress of the reaction. A crucial information is that the molecular transformation *precedes* the transformation of the crystal lattice, as clearly indicated by Figure 5. AQ guest molecules, which at the beginning of the reaction occupy substitutional sites in the DNO_2A lattice, i.e., maintain positions and orientations of the host molecules, soon reach a concentration high enough as not to allow the existence of a stable triclinic unit cell. This is possibly why, at this very moment, the energy stored in the system under stress is released and gives rise to mechanical deformations of the whole crystal, as illustrated in the right part of Figure 4. We believe that this is the step (Figure 4, picture c) when the triclinic lattice of DNO_2A is transformed into to the monoclinic lattice of AQ, whose lattice phonons soon become predominant in the Raman profiles. Therefore, the mechanical movement induced by light absorption, as shown in Figure 4, pictures c–f, provides the energetic cost of the crystal-to-crystal transformation.

3.4.4. Complete Formation of Crystalline AQ. At the final stage the AQ molecules, formerly guest molecules in the triclinic DNO_2A lattice, become themselves host molecules in a monoclinic lattice where DNO_2A molecules are now guests. This implies that, although the new crystal lattice is formed, the reaction is not complete until all reactant molecules are transformed to AQ in the AQ lattice. This would explain why in Figure 4, picture g, the crystal, which has recovered its initial

shape at time 365 min, undergoes further distortion (from picture f to g) by shrinking and bending in a fashion similar to the process previously shown in pictures a–f. Indeed, the completion of the photoreaction still requires that a sizable amount of DNO_2A molecules react and a corresponding stoichiometric amount of NO molecules leaves the crystal, which therefore shrinks to keep its cohesion. At this stage only, the reaction ends.

We must remark once again the importance of the correlation between the intramolecular vibrational spectra and the intermolecular lattice phonon spectra. This relationship is of paramount importance in probing the photochemical transformation of the molecules and, at the same time, the change of the crystal lattice.

4. MODELING THE REACTION

Now we aim to describe the transformation of DNO_2A to AQ in the solid state by emulating the experimental process, that is by first chemically transforming DNO_2A into AQ without changes to the lattice and then by continuously deforming the crystal lattice into the final AQ structure,[25] without further chemical changes and along the path with the lowest energy barrier. We must, in effect, identify the transition state, which is the minimum energy saddle point between reactants and products. To implement this program we need a model for the molecules and then a model for their interactions in the crystal.

For the molecular model we have chosen the minimum energy geometries of isolated DNO_2A and AQ molecules, determined *ab initio* with the program GAUSSIAN03,[31] using the B3LYP/6-31G* combination of density functional and basis set. The model is adequate, since the equilibrium geometries so obtained closely match the experimental molecular geometries in the crystals,[22,25] with the only noticeable difference being a small deviation (below 5°) in the C–C–N–O torsion angles in DNO_2A.

Intermolecular interactions were modeled by an atom–atom potential with electrostatic and Buckingham terms, $V_{ij}(r) = q_i q_j/r + A_{ij}\exp(-B_{ij}r) - C_{ij}/r^6$. The atomic charges q_i are the ESP charges[24] fitted to the electrostatic potential evaluated in the above-mentioned *ab initio* calculations on the isolated molecules. The A_{ij}, B_{ij}, and C_{ij} parameters for H, C, N, and O atoms are from a potential model[32] specifically designed to be internally consistent and transferable. Crystal structures were determined by seeking minimum energy lattice configurations using the WMIN program,[33] with molecules maintained rigid in their *ab initio* geometries. Several experimental and hypothetical initial lattice structures have been considered, as discussed below. The stability, or lack of stability, of the optimized structures was assessed by computing the phonon frequencies which, as a necessary and sufficient condition for local stability,[34] must be real and ≥ 0 (non-negative force constants).

As a first validation of the molecular and potential models, starting from the experimental structures[22,25] of DNO_2A (triclinic, space group $P\bar{1}$, with Z = 1) and AQ (monoclinic, space group $P2_1/a$, with Z = 2), we have determined the equilibrium configurations by minimizing the potential energy with respect to all independent structural parameters allowed by the space group symmetry. The resulting structures, hereafter labeled as D_1 and A_2, are shown in Figure 8, while their lattice parameters are listed in Table 1. The excellent agreement between calculated and experimental[22,25] parameters confirms that the models are realistic. Also excellent is the agreement between the computed binding energy of the lattice
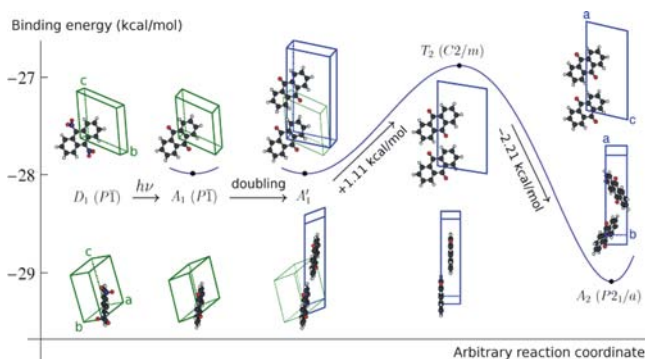
Figure 8. Reaction path from DNO_2A to AQ. D_1 is the $Z = 1$ DNO_2A structure which, when photochemically transformed to AQ, becomes the $Z = 1$ metastable structure A_1. A_1 is mathematically equivalent (through a cell doubling) to A_1', which may be transformed into the transition state T_2. Finally, T_2 spontaneously converts to A_2 (the $Z = 2$ AQ structure). Axonometric views of the various computed structures along the path are shown close to their energies. AQ and DNO_2A molecules maintain their ab initio geometries (with D_{2h} and C_{2h} symmetry, respectively) and reside on inversion sites. Graphics by MolScript.[37]

and its closest experimental equivalent, namely the sublimation enthalpy, available only for AQ.[35]

As discussed in sections 3.2 and 3.4, the photochemical molecular transformation of DNO_2A to AQ precedes the transformation of the lattice. To model this behavior, starting from the known structure of DNO_2A,[22] we have converted all DNO_2A molecules into AQ molecules and then minimized the lattice energy. We have thus reached a triclinic AQ structure with $Z = 1$ (labeled A_1), which represents a local energy minimum since all computed force constants are non-negative. This hypothetical structure, although *mechanically* stable, is predicted to be *thermodynamically* unstable, since it is less bound than the $Z = 2$ monoclinic structure A_2 (see energies in Table 1). Immediate conversion of A_1 into A_2 is hindered by the energy barrier that separates the two structures. To estimate this barrier, we have searched all possible reaction paths between A_1 and A_2. The procedure used to identify the transition state is described below and is extremely artificial. Nevertheless, we will immediately see that the resulting reaction path, illustrated in Figure 8, describes a quite obvious and easily understandable process.

The transition state, labeled T_2, is a $Z = 2$ nonprimitive monoclinic structure with space group $C2/m$. The two molecules are equivalent by translation and parallel the to ac plane. The structure, optimized with respect to all structural

parameters allowed by the monoclinic lattice, sits on an energy saddle, since some of its phonons have negative force constants. Thus, the system experiences no recall forces for displacements along these phonon modes, which describe out-of-plane molecular rotations. When first perturbed by slightly rotating the two molecules, either in the same or in opposite directions, and then optimized without constraints, the state T_2 in fact falls to either one of two different minima. One minimum (reached by rotating the two molecules in opposite directions) is identical to the (optimized) experimental AQ structure A_2. The other minimum (reached by rotating the molecules in the same direction) is a $Z = 2$ triclinic structure, labeled A_1'. It may be noticed that A_1' and A_1 have exactly the same energy. As shown in Figure 8, in fact, A_1 is just a cell halving of A_1', with cell axes $a = b'$, $b = -b' + c'$, and $c = (a' - b')/2$.

Having the trajectories from T_2 to A_1 and from T_2 to A_2, one may simply invert the first segment to obtain a composite path from A_1 to A_2. We may now fully describe the transformation, illustrated in Figure 8, from D_1 (the $Z = 1$ DNO_2A lattice) to A_2 (the $Z = 2$ AQ lattice). We first photochemically transform D_1 into A_1 (AQ in the $Z = 1$ DNO_2A lattice), which is immediately doubled into A_1', with cell axes $a' = a + 2c$, $b' = a$, and $c' = a + b$ (a purely mathematical transformation, with no effect on the energy). We then progressively deform the $Z = 2$ triclinic lattice A_1' into a monoclinic lattice, while simultaneously rotating the two molecules until they lie parallel to the ac plane. The T_2 saddle structure is thus reached, by paying an activation energy of 1.11 kcal/mol. We then rotate the two molecules in opposite directions, finally reaching the monoclinic A_2 lattice and recovering 2.21 kcal/mol, with a small net gain.

The computational procedure with which we have identified the transition state T_2 is essentially the opposite of the process just described. For the reasons discussed in section 3.4, we had deduced that the transformation from A_1 to A_2 is a cell doubling process. Several early attempts to reach a transition state by doubling A_1 (followed by optimization of the doubled structure) failed since all structures immediately reverted back to the initial A_1 structure. On retrospect, we could have predicted this, since A_1 is already a locally stable energy minimum. We may likely experimentally identify this intermediate state as the crystal arrangement of the triclinic structure with one AQ molecule per unit cell. However, in analogy with previous work,[36] direct structural evidence would require XRD time-resolved snapshots during the progress of the reaction. Halving A_2 (after rotation of the two molecules to ensure that are equivalent by translation) does not present the same problem (because by halving the cell we effectively

Table 1. Experimental and Computed Lattice Parameters[22,25] and Binding Energies[35]

Z	space group	structure	a (Å)	b (Å)	c (Å)	α (deg)	β (deg)	γ (deg)	V (Å^3)	E(kcal/mol)
					DNO_2A					
1	$P\bar{1}$	expt[17]	3.950	8.680	8.760	106.77	98.98	98.02	278.59	
		calc, D_1	3.713	8.824	8.825	105.69	98.09	98.13	270.67	−36.38
						AQ				
1	$P\bar{1}$	calc, A_1	4.157	8.258	7.778	107.74	85.60	106.30	244.08	−27.99
2	$P\bar{1}$	calc, A_1'	16.407	4.157	8.138	77.08	101.47	70.83	488.15	−27.99
2	$C2/m$	calc, T_2	15.314	3.532	9.163	90.00	98.90	90.00	489.63	−26.88
2	$P2_1/a$	expt[25,35]	15.780	3.963	7.868	90.00	102.69	90.00	480.21	−27.2 ± 4.8
		calc, A_2	16.010	3.929	7.805	90.00	102.71	90.00	478.75	−29.09

prevent the return to A_2). We have systematically tried all cell halving transformations consistent with the molecules at positions $(0,0,0)$ and $(1/2,1/2,0)$ in A_2 (see Figure 8), for a total of 504 possibilities. As expected, we have found that many transformations simply lead to different crystallographic representations of the same structure. Overall, there are only four distinct halved structures, i.e., four distinct accessible saddles around A_2, of which only one has negative energy. This specific saddle (the lowest among all saddles) is the previously discussed transition state T_2.

5. CONCLUSIONS

Solid-state reactions, being related to crystal structure modifications, are strictly mediated by lattice phonons which couple to the electronic excitation of the light field. Structure and dynamics of the crystal lattice are then equally involved, and this must be considered when setting up experiments to reveal the evolution of photoreactions. In this study we show how useful Raman spectroscopy can be to monitor both molecular and structural changes.

The photoinduced reaction of dinitroanthracene to anthraquinone fits the general picture of molecular materials that change shape and dimensions by means of the transformation of photon energy into mechanical work.[38] What we aim to emphasize most here is the mechanism underlying the crystal-to-crystal transformation, a process complicated by the need to consider all changes occurring in the molecular environment during the course of the reaction. It is self-evident that molecular changes ultimately produce modifications of the crystal lattice. Raman spectroscopy has proved to be the ideal tool to conveniently follow the evolution of the photoreaction. While analysis of the lattice modes allowed for the study of the physical changes, the chemical transformation was monitored by measuring the intramolecular Raman-active modes of both reactant and product. Working in confocal microscopy, with a Raman signal at a spatial resolution below 1 μm, has also allowed us to follow the evolution of the photoreaction *in situ* and to compare crystal and molecular spectral changes during the reaction with the microscopic optical images of the sample. The structural reconstruction required to drive the photo-reaction explains the different evolution of crystal morphology under irradiation. We have shown that a completely destructive process is observed when irradiation is produced by an intense focused laser beam, whereas a uniform distribution of the exciting radiation with a lower intensity permits a more controlled structural change. In the latter case the crystal initially keeps its shape, propagating the mechanical strain to edges and surfaces rather than undergoing cracks or breaking in small fragments.

One of the major and most surprising outcomes of this study is that molecular and lattice transformations do not proceed at the same rate. The molecular transformation precedes the structural crystal change, as illustrated in section 3.4. We emphasize the key role played by host and guest molecules which interchange in the substitutional sites of the unit cell. Former guest molecules (AQ) eventually become the host molecules and, at the same time, former host molecules (DNO_2A) take the place of guests. This is a key point when explaining the large and spectacular deformation of the crystal under irradiation.

The observed time mismatch between chemical and lattice transformation indeed allows for a clear way of modeling the crucial step of the cell doubling. In fact, once the AQ molecules

are formed inside the DNO_2A lattice, the system relaxes to a readily accessible mechanically stable structure still with $Z = 1$. From here, a local minimum, the thermodynamically stable structure with $Z = 2$ can be attained with a relatively small energy expense which leads the system through a plausible transition state.

To clarify the mechanisms underlying the relationship between incoming light and molecular constraints we have extended the study to high pressure up to 2 GPa. It was found that after 1 GPa the photoreactions becomes inhibited, since the release of NO cannot take place if the external pressure is too high. Consequently, no crystal movement is observed above 1 GPa.

The crucial point is the role played by the mechanical strain induced by light. A large structural reconstruction, as that involved in the doubling of the triclinic unit cell of DNO_2A to yield the monoclinic structure of AQ, cannot occur without striking crystal deformations accompanying the photoreaction. Light energy initially produces the chemical transformation of the molecular units in the lattice. This change induces the mechanical deformations which eventually become the driving factor of the structural change. At high pressure (>1 GPa), where crystal movements meet with molecular constraints, the photoreaction lacks its driving force and cannot reach its completion.

■ ASSOCIATED CONTENT

ⓢ Supporting Information

A Windows media video file and additional high pressure spectra. This material is available free of charge via the Internet at http://pubs.acs.org.

■ AUTHOR INFORMATION

Corresponding Author
aldo.brillante@unibo.it

Notes
The authors declare no competing financial interest.

■ ACKNOWLEDGMENTS

■ REFERENCES

(1) Craig, D. P. *J. Proc. R. Soc. New South Wales* **1982**, *61*, 115.
(2) Yoshizawa, M.; Takeyama, Y.; Okano, T.; Fujita, M. *J. Am. Chem. Soc.* **2003**, *125*, 3243.
(3) Balzani, V.; Credi, A.; Raymo, F. M.; Stoddart, J. F. *Angew. Chem., Int. Ed.* **2000**, *39*, 3348.
(4) Balzani, V.; Credi, A.; Venturi, M. *Molecular Devices and Machines: A Journey into the Nano World*; Wiley-VCH: Weinheim, 2003.
(5) Von Delius, M.; Leigh, D. A. *Chem. Soc. Rev.* **2011**, *40*, 3656.
(6) Irie, M.; Kobatake, S.; Horichi, M. *Science* **2001**, *291*, 1769.
(7) Garcia-Garibay, M. *Angew. Chem., Int. Ed.* **2007**, *46*, 8945.
(8) Morimoto, M.; Irie, M. *J. Am. Chem. Soc.* **2010**, *132*, 14172.
(9) Koshima, H.; Takechi, K.; Uchimoto, H.; Shiro, M.; Hashizume, D. *Chem. Comm* **2011**, *47*, 11423.
(10) Weder, C. *J. Mater. Chem.* **2011**, *21*, 8235 and references therein.
(11) Zhu, L.; Al-Kaisy, R. O.; Bardeen, C. J. *J. Am. Chem. Soc.* **2011**, *133*, 12569.
(12) Becker, H. D. *Chem. Rev.* **1993**, *93*, 145.
(13) Plaza-Medina, E. F.; Rodríguez-Cordoba, W.; Morales-Cueto, R.; Peon, J. *J. Phys. Chem. A* **2011**, *115*, 577.

(14) Brillante, A.; Bilotti, I.; Della Valle, R. G.; Venuti, E.; Girlando, A. *CrystEngComm.* **2008**, *10*, 937.

(15) Keating, A. E.; Garcia-Garibay, M. A. Photochemical Solid-To-Solid Reactions. In *Organic and Inorganic Photochemistry*; Ramamurthy, V., Schanze, K., Eds.; Marcel Dekker: New York, 1998; Vol. 2, p 195.

(16) Keating, A. E.; Shin, S. H.; Huang, F. K.; Garrell, R. L.; Garcia-Garibay, M. A. *Tetrahedron Lett.* **1999**, *40*, 261.

(17) Dwarakanath, K.; Prasad, P. N. *J. Am. Chem. Soc.* **1980**, *102*, 4254.

(18) Swiatkiewicz, J.; Eisenhardt, G.; Prasad, P. N.; Thomas, J. M.; Jones, W.; Theocharis, C. R. *J. Phys. Chem.* **1982**, *86*, 1764.

(19) Piermarini, G. J.; Block, S.; Barnett, J. D.; Forman, R. A. *J. Appl. Phys.* **1975**, *46*, 2774.

(20) Farina, L.; Della Valle, R. G.; Brillante, A. *High Press. Res.* **2000**, *18*, 233.

(21) Brillante, A.; Della Valle, R. G.; Farina, R.; Venuti, E. *Chem. Phys.* **1995**, *191*, 177.

(22) Trotter, J. *Acta Crystallogr.* **1959**, *12*, 232.

(23) Turrel, G. *Infrared and Raman Spectra of Crystals*; Academic Press: London, 1972.

(24) Lonsdale, K.; Milledge, K.; El- Sayed, K. *Acta Crystallogr.* **1966**, *20*, 13.

(25) Fu, Y; Brock, C. P. *Acta Crystallogr.* **1998**, *B54*, 308.

(26) Cohen, M. D.; G. M. J. Schmidt, G. M. J. *J. Chem. Soc.* **1964**, 1996.

(27) Heller, E; Schmidt, G. M. J. *Israel J. Chem.* **1971**, *9*, 449.

(28) Ramamurthy, V.; Venkatesan, K. *Chem. Rev.* **1987**, *87*, 433.

(29) Brillante, A.; Hanfland, M.; Syassen, K. *Chem. Phys. Lett.* **1985**, *119*, 42.

(30) Brillante, A.; Cau, M.; Della Valle, R. G.; Venuti, E. *Chem. Phys. Lett.* **1994**, *218*, 568.

(31) Frisch, M. J.; Trucks, G. W.; Schlegel, H. B.; Scuseria, G. E.; Robb, M. A.; Cheeseman, J. R.; Montgomery, J. A.. Jr.; Vreven, T.; Kudin, K. N.; Burant, J. C.; Millam, J. M.; Iyengar, S. S.; Tomasi, J.; Barone, V.; Mennucci, V.; Cossi, M.; Scalmani, G.; Rega, N.; Petersson, G. A.; Nakatsuji, H.; Hada, M.; Ehara, M.; Toyota, K.; Fukuda, R.; Hasegawa, J.; Ishida, M.; Nakajima, T.; Honda, Y.; Kitao, O.; Nakai, H.; Klene, M.; Li, X.; Knox, J. E.; Hratchian, H. P.; Cross, J. B.; Bakken, V.; Adamo, C.; Jaramillo, J.; Gomperts, R.; Stratmann, R. E.; Yazyev, O.; Austin, A. J.; Cammi, R.; Pomelli, C.; Ochterski, J. W.; Ayala, P. Y.; Morokuma, K.; Voth, G. A.; Salvador, P.; Dannenberg, J. J.; Zakrzewski, V. G.; Dapprich, S.; Daniels, A. D.; Strain, M. C.; Farkas, O.; Malick, D. K.; Rabuck, A. D.; Raghavachari, K.; Foresman, J. B.; Ortiz, J. V.; Cui, Q.; Baboul, A. G.; Clifford, S.; Cioslowski, J.; Stefanov, B. B.; Liu, G.; Liashenko, A.; Piskorz, P.; Komaromi, I.; Martin, R. L.; Fox, D. J.; Keith, T.; Al-Laham, M. A.; Peng, C. Y.; Nanayakkara, A.; Challacombe, M.; Gill, P. M. W.; Johnson, B.; Chen, W.; Wong, M. W.; Gonzalez, C.; Pople, J. A. *Gaussian 03*, Revision C.02; Gaussian, Inc.: Wallingford, CT, 2004.

(32) Williams, D. E.; Houpt, D. J. *Acta Crystallogr. B* **1986**, *42*, 286.

(33) Busing, W. R.; Matsui, M. *Acta Crystallogr. A* **1984**, *40*, 532.

(34) Born, M.; Huang, K. *Dynamical Theory of Crystal Lattices*; Oxford University Press: New York, 1954.

(35) Weighted average of nine published data, NIST database, http://webbook.nist.gov/.

(36) L. Zhu, L.; Agarwal, A.; Lai, J.; Al-Kaysi, R. O.; Tham, F. S.; Ghaddar, T.; Mueller, L.; Bardeen, C. J. *J. Mater. Chem.* **2011**, *21*, 6258.

(37) Kraulis, P. J. *J. Appl. Crystallogr.* **1991**, *24*, 946.

(38) Otsuka, K.; Wayman, C. M. *Shape Memory Materials*; Cambridge University Press: Cambridge, UK, 1998.